Draft March 15, 2009
Preprint typeset using LaTeX style emulateapj v. 08/13/06

SPARSE APERTURE INTERFEROMETRY WITH A NON-REDUNDANT MASK ON THE JAMES WEBB SPACE TELESCOPE

Anand Sivaramakrishnan[1,2]
Department of Astrophysics, American Museum of Natural History,
79th Street at Central Park West, New York, NY 10024

Peter Tuthill[1], Michael Ireland[1],
School of Physics, University of Sydney, NSW Australia

James P. Lloyd[1], Frantz Martinache[1]
Department of Astronomy, Cornell University, Ithaca, NY 14853

Rémi Soummer[1], Russell B. Makidon
Space Telescope Science Institute, 3700 San Martin Drive, Baltimore, MD 21218
Draft March 15, 2009

ABSTRACT

Non-redundant masking (NRM) is a high contrast high resolution technique that is relevant for future space missions dedicated to either general astrophysics or extrasolar planetary astronomy. NRM mitigates not only atmospheric but instrument-induced speckle noise as well. The recently added mask in the Fine Guidance Sensor Tunable Filter Imager (FGS-TFI) on *James Webb Space Telescope* (*JWST*) will open up a search space between 50 and 400 mas at wavelengths longer than 3.8μm. Contrast of 10^4 will be achievable in a 10 ks exposure of an $M = 7$ star, with routine observing, target acquisition, and data calibration methods. NRM places protoplanets in Taurus as well as Jovians younger than 300Myr and more massive than $2M_J$ orbiting solar type stars within *JWST*'s reach. Stars as bright as $M = 3$ will also be observable, thus meshing well with next-generation ground-based extreme adaptive optics coronagraphs. This parameter space is inaccessible to both *JWST* coronagraphs and future 30-m class ground-based telescopes, especially in the mid-IR. We show that NRM used on future space telescopes can deliver unsurpassed image contrast in key niches, while reducing mission risk associated with active primary mirrors.

Subject headings: instrumentation: interferometry — instrumentation: high angular resolution — space vehicles: instruments — techniques: high angular resolution — planetary systems

1. INTRODUCTION

Major ground-based observatories have successfully implemented non-redundant aperture-masking interferometry using existing instruments and observing procedures. Landmark discoveries such as dusty disks imaged around young stellar objects, mass-loss shells of evolved stars and the fascinating time-varying spiral plumes surrounding dusty Wolf-Rayet systems have been reported amongst the 50-odd peer-reviewed papers describing results produced by this technique (Tuthill et al. 1998; Monnier et al. 1999a,b; Tuthill et al. 2000, 2001, 2002, 2005, 2006; Lloyd et al. 2006; Pravdo et al. 2006; Martinache et al. 2007; Tuthill & Lloyd 2007; Ireland & Kraus 2008; Ireland et al. 2008; Tuthill et al. 2008). However, the atmosphere places limitations on non-redundant masking (NRM) performance.

NRM on a space telescope has not been described in the literature to date. We present detailed simulations of NRM performance on the *James Webb Space Telescope* (*JWST*) to demonstrate the exciting planetary science enabled by the recent addition of NRM to *JWST*'s suite of established instruments, and to emphasize the importance of this technique to other future space-based observatories. On *JWST* NRM will widen the telescope's science reach to include a unique combination of wavelength and angular resolution regimes inaccessible from the ground, even with the advent of extreme adaptive optics (ExAO) and coronagraphs behind 30 m extremely large telescopes of the future. For example, NRM used at 4μm will place warm extrasolar jovians within 4 to 30 AU of F, G, and K dwarfs 30pc from the Sun within *JWST*'s purview.

Indeed, NRM can add high resolution capability to large filled-aperture space telescopes without sacrificing their wide utility for general astrophysical observations. Furthermore, the NRM search space is complementary to future coronagraphic space missions dedicated to extrasolar planet imaging and characterization, as well as to ground-based ExAO instruments (Macintosh et al. 2006), in that it yields moderate contrasts between 0.5 and $4\lambda/D$ (λ being the observing wavelength, D the telescope diameter). Diffraction-limited stellar coronagraphy, on the other hand, typically covers a search space at higher contrast, at separations larger than $\sim 4\lambda/D$

[1] JWST Aperture Masking (JAM) Team
[2] Department of Physics and Astronomy, Stony Brook University, Stony Brook, NY 11794

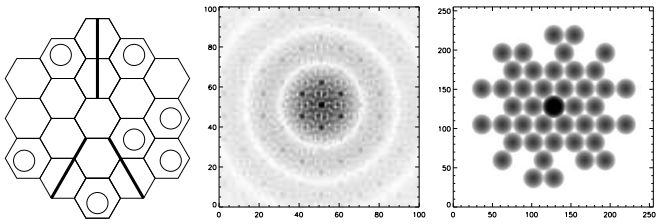

FIG. 1.— *Left:* A 7-hole non-redundant pupil mask (holes) overlaid on the *JWST* primary mirror. *Center:* A 4.05 μm FGS-TFI image of a point source, with a 1% bandwidth filter, on a negative logarithmic stretch (dark Airy rings appear white). The first Airy ring diameter is 2.4″. Generally data out to the second Airy ring is analyzed. *Right:* the power spectrum of the image (also on a negative log scale), showing fringe power on the 21 baselines passed by the mask.

(Sivaramakrishnan et al. 2001). Techniques such as Angular or Spectral Differential Imaging (e.g., Marois et al. (2006); Lafrenière et al. (2007) and references therein) do not work well at these small angular separations. In addition, NRM data has a high degree of *self-consistency* that is absent in full-aperture direct or coronagraphic imaging.

We examine the scientific merit and feasibility of NRM on *JWST*'s Fine Guidance Sensor's Tunable Filter Imager (FGS-TFI), between 3.8μm and 5μm, operating at a spectral resolution of 100. Since NRM is being implemented on *JWST*, our contrast predictions are relevant to *JWST* science planning. Our NRM designs work well in 10% bandpass filters, making NRM a possible technique for *JWST*'s near-IR imager NIRCam and mid-IR imager MIRI (Gardner et al. 2006). Our results can be scaled with both wavelength and optical path difference stability when planning NRM on future missions.

JWST's target acquisition methods, pointing stability, and data calibration pipeline processing are aimed at general purpose imaging with an undemanding operating protocol. They will suffice for the high dynamic range NRM observations we describe here. In contrast, coronagraphic observations require specialized target acquisition and peak-up (Baudoz et al. 2006), very small pointing errors (Lloyd et al. 2003), exquisite wavefront flatness and highly uniform pupil illumination (Sivaramakrishnan et al. 2001, 2005, 2008; Sivaramakrishnan et al. 2006). Lyot style coronagraphs are somewhat robust to pointing errors (Lloyd & Sivaramakrishnan 2005), but are effective only at wider angular separations. In comparison, NRM relies on long-term *stability* of the telescope's wavefront during a several minute or hour long exposure, rather than on any stringent requirements on wavefront *quality*. It therefore mitigates some of the risk associated with the complex mechanisms and sequences involved in co-phasing *JWST*'s 18-segment, deployable 6.5 m primary mirror as the telescope orbits the second Earth-Sun Lagrangian equilibrium point (e.g., Sivaramakrishnan (2006))

2. NRM INTERFEROMETRY AND ITS LIMITS

Interferometry with non-redundant baselines was developed for radio astronomy (Jennison 1958), and subsequently adapted to optical wavelengths (Baldwin et al. 1986). Today it is used in IR and optical bandpasses, often behind instruments not originally developed for sparse aperture interferometry (Tuthill et al. 1998).

Haniff et al. (1989); Readhead et al. (1988); Tuthill et al. (2000); Monnier (2003) and references therein present a fuller description of NRM. In brief, a non-redundant array of subapertures is achieved with an N-holes ($\{h_1, h_2, ..., h_N\}$) placed so no vector (baseline) between the centers of two holes is repeated (see Figure 1). The resulting PSF is created by several coherent fringe patterns (each with different angular periods on the detector, thanks to non-redundancy) overlaid across one another. A fringe formed by holes h_i and h_j is quantified by a complex visibility, which has an amplitude (degree of modulation) and a phase (the offset of the fringe's center from the centroid of the PSF). The fringe visibility is the complex product of a Fourier component of the object and a system visibility. Therefore, when observing a point-source, this phase ϕ_{ij} measures the piston wavefront error between the two holes. A *closure phase* is formed by the addition of three fringe phases created by a triangle of holes, $\{h_i, h_j, h_k\}$, notably $\phi_{ij} + \phi_{jk} + \phi_{ki}$. Although piston wavefront errors change the fringe phases, the closure phases are insensitive to these wavefront errors and only measure source structure. There are $N(N-1)(N-2)/6$ independent closure phases measurable in the image.

NRM is a form of *imaging* with a PSF that looks unusual. The NRM PSF displays multiple sharp peaks, whereas traditional diffraction-limited PSFs are dominated by one peak. However, the NRM PSF possesses some useful properties. First, through the use of closure phase, it is insensitive to large scale wavefront errors over the pupil. Second, its core is more than twice as narrow as a traditional PSF's (the Michelson criterion, $0.5\lambda/D$, cf. Rayleigh's criterion, $1.22\lambda/D$). Third, NRM data sets produce results that can be averaged to reduce noise, even in the presence of slowly-varying speckles. By comparison, co-adding PSFs in the presence of speckle noise is always limited by a speckle noise floor (Sivaramakrishnan et al. 2002; Soummer et al. 2007a).

On the ground NRM filters out aberrations that pass through an AO system. It is insensitive to the non-common path (NCP) aberrations between the science and sensing arms of the instrument. The NCP issue has only recently been addressed by specialized calibration systems in future ExAO coronagraphic systems utilizing full-aperture pupils (Sivaramakrishnan et al. 2008). Today's ground-based NRM routinely achieves stability of 0.5 degrees on the closure phase, hence passively stabilizing the phase at the level of $\lambda/500$ to $\lambda/1000$.

For a point source any closure phase must be zero. A measured non-zero closure phase in the data provides spatial information on the object. A consistent, systematic, instrument-induced departure from a zero closure phase can be measured using a calibration star, and subtracted from a target's closure phase. Conceptually, closure phase data analysis is a model fit of the intensity distribution on sky, the observations being closure phases from all the closed triangles that can be constructed with the given set of baselines. Fringe visibility data makes solving for the actual image (or its measured Fourier components) possible. The inner working angle (IWA) of such an image is $0.5\lambda/D$, the outer working angle (OWA) is set by the shortest baseline available. Recovering the measured Fourier components of source structure with NRM imaging using both closure phases

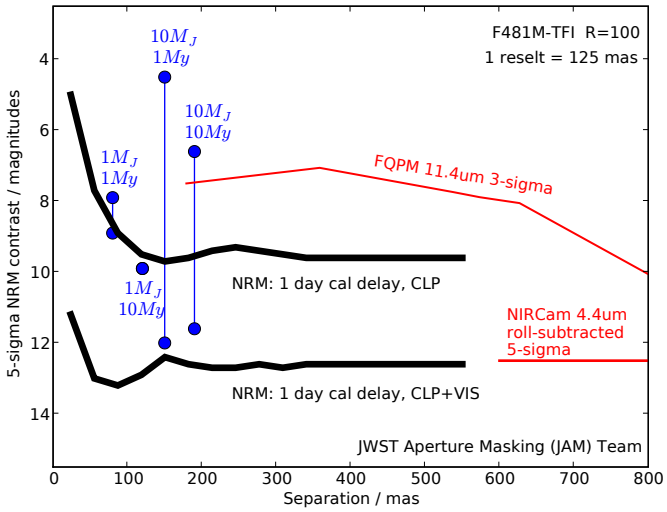

FIG. 2.— A comparison of predicted *JWST* NRM and coronagraph performance. Estimated dynamic range using only closure phase (CLP) as well as closure phase in combination with fringe visibility (CLP+VIS) data for 1% bandpass NRM imaging at 4.81μm using the 7-hole mask (shown in Figure 1) in *JWST*'s FGS Tunable Filter Imager (TFI) is plotted. A one day delay between target star and calibrator is modeled using worst-case attitude-dependent thermal changes. Guiding errors and intra-pixel sensitivity are also simulated. Photon noise sets a limit of dynamic range of 10 magnitudes with a 10ks exposure on an M=7 target . 10% bandwidths will produce similar results with 1ks exposures. The range of estimated contrasts between a solar type star and 1 and 10 Jupiter mass planets, at ages of 1 and 10 Myr (Baraffe et al. 2003; Marley et al. 2007) are shown in blue (at arbitrary separations). This configuration can detect protoplanets in Taurus. The same mask *JWST* NIRCam would produce 1 to 2 magnitudes less contrast at 2 μm, but at half the corresponding angular separation. Such a mask in MIRI could produce better contrast, though the useful field of view scales with wavelength. At 4.8 μm NRM performance drops outside about 600mas. The NIRCam linear band-limited coronagraph performance (Krist et al. 2007), plotted in red, complements the FGS-TFI NRM search space. The most optimistic *JWST* MIRI four quadrant phase mask coronagraph 11 μm contrast curve with a fixed 5mas pointing error, no guiding error, and no error in calibration star placement is also plotted in red (Cavarroc et al. 2008).

and fringe visibilities is a well-posed problem. This is not the case with full aperture imaging. Ground-based fringe visibilities suffer from temporal instabilities due to atmospheric scintillation and transparency variations. On *JWST* fringe visibilities should be stable since segment reflectivity is unlikely to vary perceptibly during a single exposures, or between science and calibrator exposures.

In practice dynamic range may be limited by effects such as a non-isotropic guiding error, detector flat field errors, and pupil wander. Target placement repeatable to an arcsecond on *JWST*'s HAWAII-2RG detectors will improve data calibration, given the spatial frequency of the detector' flat field structure (Figer et al. 2004).

3. NRM IN SPACE

Without AO, ground-based NRM, like speckle interferometry, must freeze temporally-varying fringe patterns. AO stabilizes relative piston differences between subapertures in the aperture mask. This enables longer exposure times, limited by pixel well-depth, thermal background rates or instrument stability. Once deployed, *JWST*'s primary mirror segments' positions relative to each other are expected to drift slowly. Exposure times will likely be limited by cosmic rays, with a maximum single exposure time measured in hours. Under such conditions, NRM opens up a search space completely beyond the reach of ground-based telescopes. Thermal background and atmospheric opacity also limit ground-based imaging longward of about 2μm. Furthermore, *JWST*'s unusual primary mirror geometry and articulation are unlikely to cause any problems for NRM interferometry.

For a 0.5m^2 subaperture at 4μm, a 1% filter bandwidth and 50% net quantum efficiency, $M \simeq 7$ is the limit for 10^4 contrast in 10ks, and $M = 12$ the limit for 10^3 contrast in 10ks. Using a 10% bandwidth filter will reduce exposure times by a factor of ten for the same contrast. At bandwidths in excess of 10% the contrast of our mask designs starts to degrade. FGS-TFI sub-array readouts will enable observations of $M = 3$ objects.

4. SIMULATIONS

We used ten Monte Carlo realizations of *JWST*'s wavefront that conform to *JWST*'s wavefront error budget (Lightsey et al. 2004). These realizations yield PSFs at 2μm with Strehl ratios above 80%. They are estimates, given the expected residual wavefront error 14 days after active tuning of the *JWST* primary mirror (PM) figure has been performed, and the telescope slewed from a spacecraft attitude with the most thermal load from the Sun to one with the least such thermal load. To preserve the individual segment wavefront errors associated with one realization of the 18 segments in *JWST*'s PM, we extracted the individual segment piston errors from each of the ten wavefront maps, and used them to create ten instances of a single thermally perturbed set of PM segments.

Using methods described in Sivaramakrishnan et al. (2003, 2004); Soummer et al. (2007b); Makidon et al. (2008), we simulated images on a 9-fold finer grid than the 65 mas FGS-TFI detector pixel pitch. We dithered the oversampled PSFs by one sample spacing to model pointing errors of 7mas per axis. Intra-pixel quantum efficiency was modeled as a quadratic, ranging from unity at a pixel center to 0.8 at a pixel corner. We then binned the 9×9 dithered subsampled PSFs to create an image on the FGS-TFI pixel scale. We did not explicitly simulate photon noise, read out noise ($\sim 15e^-$ rms for a double-correlated sample), or detector flat field errors, although our detection threshold calculations have taken some account of these processes.

Simulated data were analyzed with a pipeline used for Keck, Palomar, and VLT data. (e.g., Kraus et al. (2008)). Nine of the ten PSF realizations in a set were taken to be calibrator observations, and one of the ten was taken to be the target observation. This process was repeated for several choices of target PSF. Rather than replicating the complex Monte-Carlo process of Kraus et al. (2008), we chose to use a simple detection threshold of 5σ, with closure-phase and visibility standard deviations calculated from scatter within the 9 calibrator observations. Note that typical 99.9% detection thresholds in Kraus et al. (2008) were $\sim$4 to 4.5σ with a more complete Monte-Carlo, which was verified by the lack of numerous false detections in that paper. We therefore believe our 5σ limit is conservative.

Figure 2 shows the contrast achieved with dynamic range calculated two ways: first, using only the closure phases (labelled CLP) for a comparison with current ground-based results, and second, using both closure phases and fringe visibilities (labelled CLP+VIS), to estimate the full range of contrast available to *JWST*. Contrast between M_J and $10M_J$ planets 1 and 10 Myr old and a parent G2V dwarf are shown in the figure. We find our mask designs produce these estimated contrasts even when the detector's pixel pitch is slightly worse than Nyquist. The very highest contrast shown is obtained using both closure phases as well as visibilities.

Dithering and drizzling images (Koekemoer 2006) may further enable undersampled data recovery. Information from routine wavefront sensing observations (Makidon et al. 2008) may help improve the dynamic range of NRM data. We have not examined these two refinements.

5. BENEFITS OF NRM IN SPACE

NRM brings both scientific and operational advantages to *JWST*, given the telescope's segmented architecture (Sivaramakrishnan et al. 2003; Sivaramakrishnan, A. 2004; Long 2006). Every NRM image measures the relative piston between each hole in the aperture mask, with a capture range set by the filter coherence length. Images taken through two masks with ∼5% throughput can measure segment pistons and tilts to interferometric precision, without any segment movement or PSF degradation. Coarse co-phasing *JWST* can be accomplished using 1% bandpass filters and NRMs. Masks in separate cameras mitigate instrument failure-induced risk, and enables campaign mode observing with the best image quality possible in any camera equipped with two NRM's. Two such masks in a camera can measure its field-dependent and chromatic aberrations. Camera-specific wavefront knowledge can feed into data reduction, benefiting science that requires thorough understanding of temporal, spatial, and chromatic variations in the PSF. In addition, NRM observations determine stellar multiplicity at the highest resolution and contrast possible. Such observations can eliminate inappropriate wavefront sensing or guide star choices. Images taken as the pupil is stepped across the mask (or vice versa) will measure pupil location without specialized pupil imaging optics. Such information is relevant for IR instrument and telescope maintenance.

6. CONCLUSION

Detailed simulations with time-varying mirror figure errors and existing data reduction methods suggest that placing a non-redundant aperture mask on any of the *JWST* instruments brings exciting high resolution high contrast imaging within reach. The 7-hole NRM in the Fine Guidance Sensor's Tunable Filter Imager will image protoplanets in Taurus. Such aperture masking provides *JWST* with alternative, risk-reducing wavefront measuring techniques, while increasing the science output of *JWST* substantially, and paving the way for future missions with NRM instrumentation. Future missions can increase the science payoff with more optimized NRM modes, making the technique interesting for galactic, extragalactic, and cosmological observations.

We thank R. Doyon, P. A. Lightsey, J. C. Mather and M. Robberto for encouraging discussions and helpful information. This work is supported in part by the National Science Foundation under Grant AST 08-04417.

REFERENCES

Baldwin, J. E., Haniff, C. A., Mackay, C. D., & Warner, P. J. 1986, Nature, 320, 595
Baraffe, I., Chabrier, G., Barman, T. S., Allard, F., & Hauschildt, P. H. 2003, A&A, 402, 701
Baudoz, P., Boccaletti, A., Riaud, P., Cavarroc, C., Baudrand, J., Reess, J. M., & Rouan, D. 2006, PASP, 118, 765
Cavarroc, C., Boccaletti, A., Baudoz, P., Amiaux, J., & Regan, M. 2008, PASP, 120, 1016
Gardner et al. 2006, Space Science Reviews, 123, 485
Haniff, C. A., Buscher, D. F., Christou, J. C., & Ridgway, S. T. 1989, MNRAS, 241, 51P
Ireland, M. J., Kraus, A., Martinache, F., Lloyd, J. P., & Tuthill, P. G. 2008, ApJ, 678, 463
Ireland, M. J. & Kraus, A. L. 2008, ApJ, 678, L59
Jennison, R. C. 1958, MNRAS, 118, 276
Koekemoer. 2006, JWST-STScI-000647
Kraus, A. L., Ireland, M. J., Martinache, F., & Lloyd, J. P. 2008, ApJ, 679, 762
Krist, J. E., Beichman, C. A., Trauger, J. T., Rieke, M. J., Somerstein, S., Green, J. J., Horner, S. D., Stansberry, J. A., Shi, F., Michael R. Meyer, M. M., Stapelfeldt, K. R., & Roellig, T. L. 2007, in Proc. SPIE, ed. D. R. Coulter, Vol. 6693, 66930H
Lafrenière, D., Doyon, R., Nadeau, D., Artigau, É., Marois, C., & Beaulieu, M. 2007, ApJ, 661, 1208
Lightsey, P. A., Barto, A. A., & Contreras, J. 2004, in Proc. SPIE, ed. J. C. Mather, Vol. 5487, 825–832
Lloyd, J. P., Martinache, F., Ireland, M. J., Monnier, J. D., Pravdo, S. H., Shaklan, S. B., & Tuthill, P. G. 2006, ApJ, 650, L131
Lloyd, J. P. & Sivaramakrishnan, A. 2005, ApJ, 621, 1153
Lloyd et al. 2003, in Proc. SPIE, ed. A. B. Schultz, Vol. 4860, 171–181
Long, K. S. 2006, JWST-OPS-002018 , revision B
Macintosh et al. 2006, in Proc. SPIE, ed. B. Ellerbroek and D. Bonaccini, Vol. 6272
Makidon et al. 2008, in Proc. SPIE, Vol. 7010, 70100
Marley, M. S., Fortney, J. J., Hubickyj, O., Bodenheimer, P., & Lissauer, J. J. 2007, ApJ, 655, 541
Marois, C., Lafrenière, D., Doyon, R., Macintosh, B., & Nadeau, D. 2006, ApJ, 641, 556
Martinache, F., Lloyd, J. P., Ireland, M. J., Yamada, R. S., & Tuthill, P. G. 2007, ApJ, 661, 496
Monnier, J. D. 2003, Reports of Progress in Physics, 66, 789
Monnier, J. D., Tuthill, P. G., & Danchi, W. C. 1999a, ApJ, 525, L97
Monnier, J. D., Tuthill, P. G., Lopez, B., Cruzalebes, P., Danchi, W. C., & Haniff, C. A. 1999b, ApJ, 512, 351
Pravdo, S. H., Shaklan, S. B., Wiktorowicz, S. J., Kulkarni, S., Lloyd, J. P., Martinache, F., Tuthill, P. G., & Ireland, M. J. 2006, ApJ, 649, 389
Readhead, A. C. S., Nakajima, T. S., Pearson, T. J., Neugebauer, G., Oke, J. B., & Sargent, W. L. W. 1988, AJ, 95, 1278
Sivaramakrishnan, A. 2006, JWST-STScI-000957
Sivaramakrishnan, A., Koresko, C. D., Makidon, R. B., Berkefeld, T., & Kuchner, M. J. 2001, ApJ, 552, 397
Sivaramakrishnan, A., Lloyd, J. P., Hodge, P. E., & Macintosh, B. A. 2002, ApJ, 581, L59
Sivaramakrishnan, A., Makidon, R. B., Acton, D. S., & Shi, F. 2003, JWST-STScI-000341
Sivaramakrishnan, A., Soummer, R., Pueyo, L., Wallace, J. K., & Shao, M. 2008, ApJ, 688, 701
Sivaramakrishnan, A., Soummer, R., Sivaramakrishnan, A. V., Lloyd, J. P., Oppenheimer, B. R., & Makidon, R. B. 2005, ApJ, 634, 1416
Sivaramakrishnan, A. 2004, JWST-STScI-000378

Sivaramakrishnan et al. 2003, in Proc. SPIE, ed. J. C. Mather, Vol. 4850, 388–397
Sivaramakrishnan et al. 2004, in Proc. SPIE, ed. J. C. Mather, Vol. 5487, 909–917
Sivaramakrishnan et al. 2006, in IAU Colloq. 200: Direct Imaging of Exoplanets: Science & Techniques, ed. C. Aime & F. Vakili, 613–616
Soummer, R., Ferrari, A., Aime, C., & Jolissaint, L. 2007a, ApJ, 669, 642
Soummer, R., Pueyo, L., Sivaramakrishnan, A., & Vanderbei, R. J. 2007b, Optics Express, 15, 15935
Tuthill, P., Monnier, J., Tanner, A., Figer, D., Ghez, A., & Danchi, W. 2006, Science, 313, 935
Tuthill, P. G. & Lloyd, J. P. 2007, Science, 316, 247
Tuthill, P. G., Monnier, J. D., & Danchi, W. C. 2001, Nature, 409, 1012
—. 2005, ApJ, 624, 352
Tuthill, P. G., Monnier, J. D., Danchi, W. C., Hale, D. D. S., & Townes, C. H. 2002, ApJ, 577, 826
Tuthill, P. G., Monnier, J. D., Danchi, W. C., & Haniff, C. A. 1998, in Proc. SPIE, ed. R. D. Reasenberg, Vol. 3350, 839–846
Tuthill, P. G., Monnier, J. D., Danchi, W. C., Wishnow, E. H., & Haniff, C. A. 2000, PASP, 112, 555
Tuthill, P. G., Monnier, J. D., Lawrance, N., Danchi, W. C., Owocki, S. P., & Gayley, K. G. 2008, ApJ, 675, 698